LINEAR FREQUENCY MODULATION INFRARED THERMAL IMAGING DETECTION TECHNOLOGY FOR GFRP/PMI FOAM SANDWICH STRUCTURE DEFECTS

by

Ya-Fei SONG[a], Qing-Ju TANG[a*], Chi-Wu BU[b], Yu-Mei LU[a], and Peng XU[a]

[a]School of Mechanical Engineering, Heilongjiang University of Science and Technology, Harbin, China
[b]College of Light Industry, Harbin University of Commerce, Harbin, China

Original scientific paper
https://doi.org/10.2298/TSCI220806007S

As one of the important structures of composite materials, polymethacrylimide (PMI) foam sandwich structure is prone to debonding and delamination defects during manufacturing and service, which seriously affects the mechanical properties of materials. Therefore, it is necessary to detect the defects of foam sandwich structure. A linear frequency modulation infrared thermal wave nondestructive testing system was built to study the correlation between the geometric characteristics (diameter and depth) of the defect and the surface temperature signal and its influence on the detection effect. The image sequence is processed by principal component analysis, discrete Fourier transform, thermal wave signal reconstruction, and other algorithms. Studies have shown that the larger the defect diameter, the shallower the depth, easy to detect defects, detection effect is good. The detection system can effectively detect and identify debonding and delamination defects. The thermal wave signal reconstruction method is superior to the principal component analysis method and the discrete Fourier transform method in the signal-to-noise ratio index, which improves the quality of the image and is conducive to the effective identification of the image surface defect information.

Key words*: PMI foam sandwich structure, linear frequency modulation, image sequence processing, signal to noise ratio*

Introduction

Advanced foam cores such as PMI foams [1, 2]. It is widely used in aerospace, medical equipment, radar antenna covers and other fields because of its light weight, high specific stiffness, good heat preservation and heat insulation performance, and the ability to meet the use requirements under specific conditions by selecting appropriate panels, core materials and adhesives [3]. The PMI foam sandwich structure has many steps in the production process, the process is complex, and the service environment is relatively harsh, the composite layer between the foam and the skin is prone to curing, resulting in defects such as delamination and debonding. Seriously affect the mechanical properties of materials. If the

*Corresponding author, e-mail: tangqingju@126.com

material defects cannot be accurately and reliably detected, the development of defects will affect the service life of the material and even threaten the safety of human life. Therefore, it is necessary to detect the defects of foam sandwich structure effectively [4].

Infrared thermal wave non-destructive testing is a new detection technology [5]. Compared with conventional detection technology, it has the characteristics of non-contact, fast detection speed, large area, high detection accuracy and intuitiveness. It is widely used in aerospace, railway, medical, mechanical, petrochemical and other fields.

In this paper, the excitation method of linear frequency modulation (LFM) infrared thermal wave non-destructive testing is used to detect the PMI foam sandwich specimens with debonding and delamination defects. The LFM infrared thermal wave non-destructive testing system is built. The correlation between the geometric characteristics of the defects and the surface temperature signal and the influence on the detection effect are studied. The image sequence is processed by three algorithms: principal component analysis (PCA), discrete Fourier transform, and thermal wave signal reconstruction (TSR). The signal-to-noise ratio (SNR) is defined to measure the effect of three algorithms on the feature extraction of PMI foam sandwich defects.

The LFM infrared thermal wave non-destructive testing system

Test system

The LFM infrared thermal imaging is an active infrared thermal imaging using a LFM signal. The advantage is that the thermal excitation is applied to the specimen through a variable frequency, which overcomes the shortcomings of the traditional infrared lock-in thermal imaging that can only detect the corresponding diffusion depth defects with a single modulation, and can effectively detect the shape and size of defects in different depth ranges [6]. Figure 1 shows the construction of infrared thermal wave non-destructive testing system. The test system is mainly composed of three parts: excitation system, acquisition system, and image sequence processing. The heat flow of LFM, mainly composed of static and dynamic components, is given as [7]:

$$q(t) = q_s + q_D = \frac{q_{\max}}{2}\left\{1+\sin\left[2\pi\left(f_0 + \frac{f_e - f_0}{2T}t\right)t\right]\right\}, \quad t \in [0,T] \tag{1}$$

where $q(t)$ represents the surface heat flux, $q_{\max}$ – the surface heat flux peak, q_s – the static component of heat flow, q_D – the dynamic component of heat flow, f_0 – the initial frequency, f_e – the termination of the frequency, T – the scan period, and t – the actuation time.

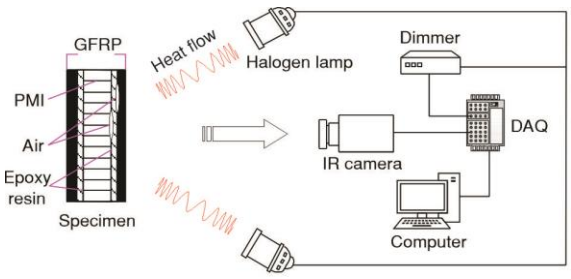

Figure 1. Infrared thermal wave NDT test system

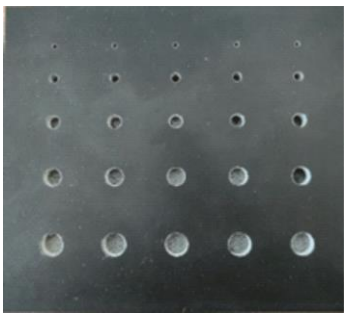

Figure 2. Schematic diagram of PMI foam sandwich structure

Test equipment

The specimen is made of PMI foam interlayer and upper and lower GFRP skin bonded by binder epoxy resin. Its size is 160 mm × 140 mm × 6.5 mm. Figure 1 is the infrared thermal wave NDT test system. Figure 2 is a schematic diagram of PMI foam sandwich structure.

Influence of defect geometric characteristics

Effect of defect diameter

Under the conditions of output power, starting frequency, termination frequency, acquisition time and sampling frequency of 1600 W, 0.1 Hz, 0.05 Hz, 20 seconds, and 20 Hz respectively, the relationship between different diameters (10 mm, 8 mm, 6 mm, and 4 mm) and temperature difference is obtained, as shown in fig. 3(a). Figure 3(b) is the first peak temperature difference trend diagram corresponding to different diameters.

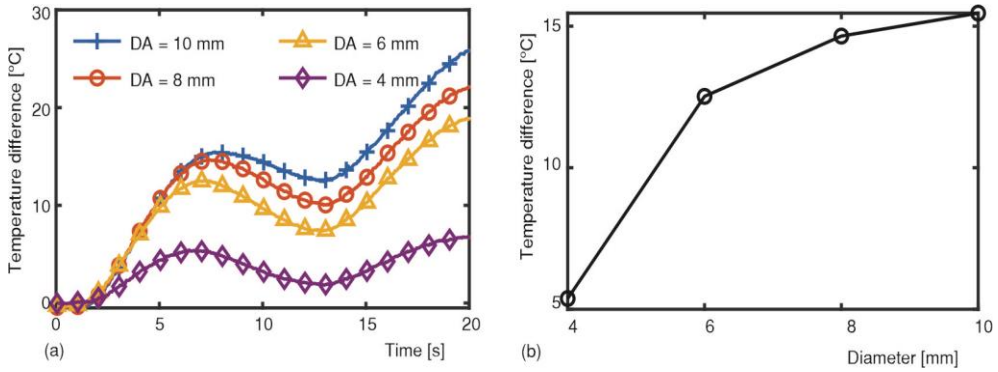

Figure 3. Effect of defect diameter

It can be seen from the figure that the temperature difference corresponding to the defect area increases first, then decreases and then increases with the action of the excitation time. In the case of the same defect depth, the temperature difference at the defect is obvious with the increase of the defect diameter, and the corresponding surface temperature difference is larger. The first temperature difference peak corresponding to the defect diameter increased from 4 mm to 10 mm also increased from about 5 to about 15. The increase in defect size further hindered the heat transfer inside the specimen, so that most of the heat was accumulated at the defect. Studies have shown that in the case of the same defect depth, the larger the defect diameter, the greater the temperature difference at the defect, the more easily detected defects.

The influence of defect depth

Under the conditions of output power, starting frequency, termination frequency, acquisition time and sampling frequency of 1600 W, 0.1 Hz, 0.05 Hz, 20 seconds and 20 Hz, the relationship between different depths (0.5 mm, 0.8 mm, 1.0 mm, 1.1 mm) and temperature difference is obtained, as shown in fig. 4(a). Figure 4(b) is the first peak temperature difference trend diagram corresponding to different depths.

It can be seen from the figure that the temperature difference corresponding to the defect area increases first, then decreases and then increases with the effect of excita-

tion time. In the case of the same defect diameter, the shallower the defect depth, the more obvious the temperature difference at the defect, and the larger the corresponding surface temperature difference. The first peak temperature difference corresponding to the change of the buried depth of the defect from 1.1 mm to 0.5 mm also increased from about 2 to about 15 ; the shallower the buried depth of the defect, the easier it is to obtain heat, and the less heat is lost when the heat is transferred inside the specimen. Studies have shown that in the case of the same defect diameter, the shallower the depth of the defect, the greater the temperature difference at the defect, the more easily the defect is detected.

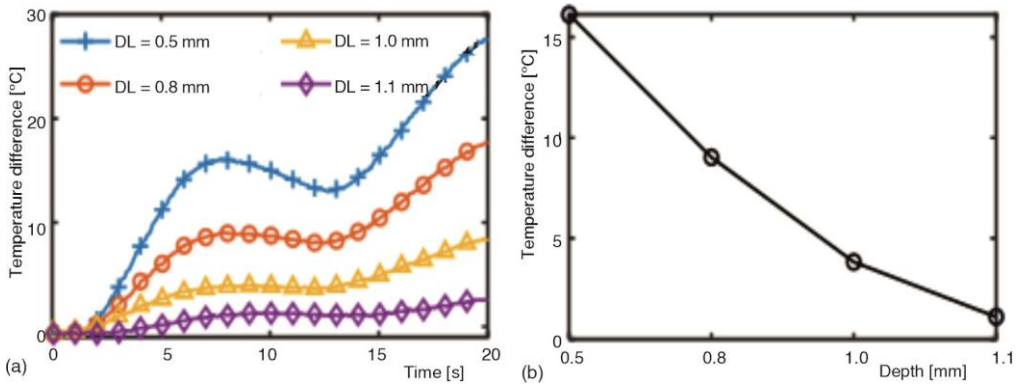

Figure 4. Effect of defect depth

Image sequence processing

Principal component analysis

The PCA is a widely used data dimension reduction algorithm [8]. The steps of the algorithm are:

- The heat map sequence composed of N frames of images is transformed into an $m \times n$ dimensional matrix A. Figure 5(a) shows the time component A_1, which is composed of $n_x \times n_y$ rows and N columns. Figure 5(b) shows the spatial component, which is composed of N rows and $n_x \times n_y$ columns.
- Make the difference between each row vector in matrix A and the average vector A_{mean} extracted from it is used to suppress noise.
- Solve the covariance matrix obtained by $A - A_{\text{mean}}$ or perform singular value decomposition on it.
- The principal components that can reflect most of the feature information of the image sequence are selected from the feature vectors by sorting the contribution rate.

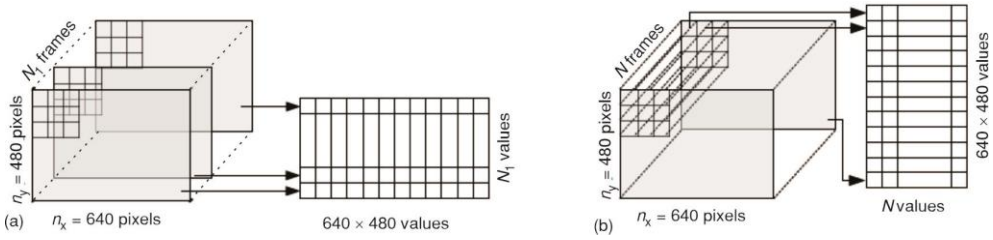

Figure 5. Schematic diagram of PCA; (a) time component and (b) space component

Discrete Fourier transform (DFT)

The DFT is analyzed from the perspective of frequency domain. The signal is transformed from the original time domain to the frequency domain, and the signal is regarded as the superposition of many signals. The frequency characteristics, namely the amplitude and phase information of the signal, can be obtained. Fourier transform is performed on the temperature signal of each pixel in the image sequence collected by infrared thermal imager [9]. This implies that:

$$F_n = \sum_{k=0}^{N-1} \alpha(k) e^{-j2\pi nk/N} = R_n + jI_n \tag{2}$$

where $\alpha(k)$ is the temperature value at pixel (x,y) on heat map, n – the serial number after discrete frequency, and R_n and I_n are the real and imaginary parts of the complex number.

Equation (2) is used to calculate the amplitude and phase of n frequency. Here, we show:

$$A(n) = \sqrt{R_n^2 + I_n^2} \quad \text{and} \quad \phi(n) = \arctan\left(\frac{I_n}{R_n}\right) \tag{3}$$

Thermal signal reconstruction

Thermal signal reconstruction (TSR) uses synthetic signal technology to reconstruct signals [10]. The TSR processes the time series of each individual pixel and transforms the time response data into logarithmic domain for linearization. Thus, we have:

$$\ln\left[\Delta T_S(t)\right] = \ln\left(\frac{q_0}{e}\right) - \frac{1}{2}\ln(\pi n) \tag{4}$$

where $\Delta T_S(t)$ is the temperature difference before and after surface heating and t is the time.

If image sequence can be reconstructed by the least square method, we get:

$$\ln\left[\Delta T_S(t)\right] = \sum_{n=0}^{N} a_n \left[\ln(t)\right]^n \tag{5}$$

If we take e index of the previous formula for data reconstruction, then we present:

$$\Delta T_S(t) = \exp\left(\sum_{n=0}^{N} a_n \left[\ln(t)\right]^n\right) \tag{6}$$

$$\frac{\Delta T_S(t)}{\mathrm{d}t} = \exp\left(\sum_{n=0}^{N} n a_n \left[ln(t)\right]^{n-1}\right) \tag{7}$$

$$\frac{d^2 \Delta T_S(t)}{\mathrm{d}t^2} = \exp\left(\sum_{n=0}^{N} n(n-1) a_n \left[ln(t)\right]^{n-1}\right) \tag{8}$$

Comparison of different algorithms in image sequence processing

In order to satisfy that the data under each parameter can be compared with each other on the same magnitude, all the data are normalized. Thus, we show:

$$p = \frac{p_0 - p_{\min}}{p_{\max} - p_{\min}} \tag{9}$$

where p is the normalized experimental data, p_0 – the original data, $p_{\min}$ – the minimum value of p_0, and $p_{\max}$ – the maximum in p_0.

The signal-to-noise ratio (SNR) [11] is defined as the evaluation standard of image quality and the influence of different parameters on defect detection is measured. The expression is shown in eq. (10). Thus, we get:

$$SNR = \frac{\left|\overline{p_d} - \overline{P_s}\right|}{\sigma_s} \tag{10}$$

where $\overline{p_d}$ is the mean value of crack zone feature, $\overline{P_s}$ – the mean value of features in the crack-free region, σ_s – the standard deviation of eigenvalue in crack-free area, and SNR is the signal-to-noise ratio.

The images with the largest SNR obtained after using three algorithms: PCA, discrete Fourier transform (DFT) method, and TSR method are shown in fig. 6(a)-6(f) are 2-D diagrams of PCA, DFT amplitude, phase, TSR exponential fitting, first-order and second-order.

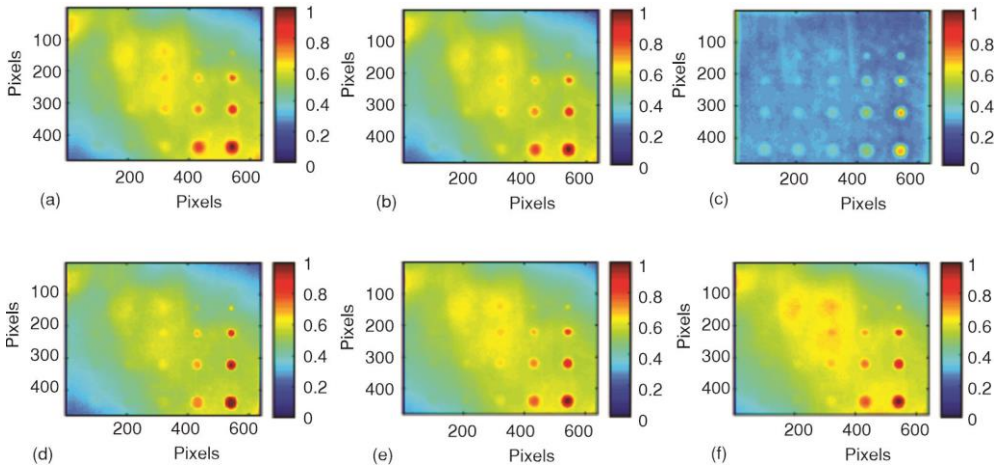

Figure 6. Processing diagram of various algorithms; (a) PCA-2-D, (b) DFT-2-D amplitude, (c) DFT-2-D phase, (d) TSR-2-D exponential fitting, (e) TSR-2-D first-order, and (f) TSR-2-D second-order

Image sequence is processed by different feature extraction algorithms, and the results are different. In order to evaluate the detection and recognition effect of PCA, DFT, and TSR image sequence processing algorithms on the debonding defects of PMI foam sandwich structure specimens, normalized images processed by the algorithm were processed and quantitative evaluation is carried out by the SNR. The results show that the original image is significantly improved after PCA algorithm processing, the clarity of defects is displayed in different colors, the difference between defect areas and defect areas is large, and the signal-to-noise ratio is large. The larger the defect diameter and the smaller the depth, the more prominent the defect. After DFT processing compared with PCA, the noise effect in amplitude figure is reduced, the SNR increases, can be seen from the defect of the third column defect edge diffusion effect is better than that of the principal component, defect is relatively clear, Fourier amplitude figure than phase diagram affected by noise is small, but the defect of phase diagram shows clearer and geometric feature is more obvious. Compared with the other two methods, the TSR algorithm can filter a large amount of noise interference, and the defect edge area is clear, the geometric characteristics are more obvious, and the SNR is the highest.

Figure 7(b) shows the SNR calculated according to the calculation method previously defined. It can be seen from the intuition and evaluation indexes of the image processed by the algorithm that the TSR method has better extraction effect on defect features and is more conducive to defect identification.

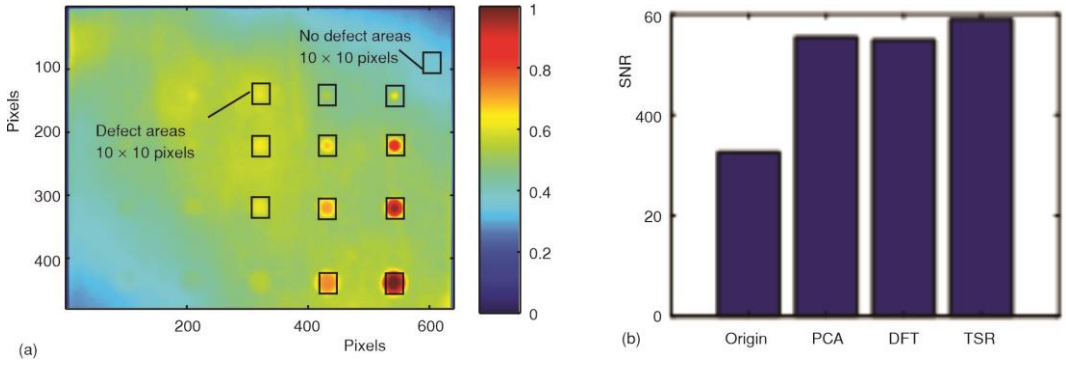

Figure 7. Region selection and Calculation of SNR

Conclusion

Aiming at the debonding defects of GFRP/PMI foam sandwich structure during service, a LFM infrared thermal wave non-destructive testing system was built. The relationship between the geometric characteristics (diameter and depth) of the defect and the surface temperature signal and its influence on the detection effect were studied. The image sequence is processed by PCA, DFT, TSR, and other algorithms. Studies have shown that the larger the defect diameter, the shallower the depth, easy to detect defects, detection effect is good. The TSR method is superior to the PCA method and the DFT method in the SNR index, which improves the quality of the image and is conducive to the effective identification of the image surface defect information.

Acknowledgment

This project is supported by National Natural Science Foundation of China (Grant No. 51775175), Heilongjiang Provincial Undergraduate University Funded Project of Basic Scientific Research Business Fee (Grant No. 2020-KYYWF-0696), and Heilongjiang Province Natural Science Fund (Grant No. LH2021E088).

References

[1] Cao, W. Y., *et al*., Development and Prospect of High Performance Polymer Composites in China, *Engineering Sciences in China*, *22* (2020), 5, pp. 112-120
[2] Xu, Z., *et al*., The Research Progress of Foam Sandwich Structure Composite Material, *Aging and Application of Synthetic Materials*, *45* (2016), 4, pp. 96-99
[3] Zhou, J. L., *et al*., The Effects of Microcell Structure on Quasi-static Compression Performance of PMI Foam, *Materials Review*, *31* (2017), 20, pp. 147-151
[4] Hu, P., *et al*., Non-destructive Test Methods of PMI Foam Cored Composite Sandwich Structures, *Materials Engineering*, *S2* (2009), June, pp. 354-358
[5] Tang, Q. J., *et al*., Theoretical Study on Infrared Thermal Wave Imaging Detection of Semiconductor Silicon Wafers with Micro-crack Defects, *Thermal Science*, *24* (2020), 6B, pp. 4011-4017
[6] Liu, Y. L., *et al*., Numerical Simulation of Infrared Thermal Wave Detection of Defects in Thermal Barrier Coatings by Linear Frequency Modulation Continuous Optical Excitation, *Journal of Heilongjiang University of Science and Technology*, *28* (2018), 5, pp. 537-542

[7] Tang, Q. J., *et al*., Infrared Micro Thermal Imaging Detection of Micro-crack Defects in Semiconductor Silicon Wafers, *Journal of Heilongjiang University of Science and Technology*, *31* (2021), 2, pp. 177-183
[8] Sun, Q. L., *et al*., Image Segmentation Based on Principal Component Analysis, *Journal of Taiyuan University of Technology*, *49* (2018), 5, pp. 759-764
[9] Ma, Y. H., *et al*., Discrete Fourier Transform and its Application, *Chinese Modern Educational Equipment*, (2015), 13, pp. 56-58
[10] Shepard, S. M., *et al*., Enhancement and Reconstruction of Thermographic NDT Data, *Proceedings of Spie the International Society for Optical Engineering*, *4710* (2002), 3, pp. 531-535
[11] Gong, J. L., *et al*., A Study on the SNR Performance Analysis of Laser-generated Bidirectional Thermal Wave Radar Imaging Inspection for Hybrid C/GFRP Laminate Defects, *Infrared Physics & Technology*, *111* (2020), 7, pp. 103526

Paper submitted: August 6, 2022
Paper revised: November 15, 2022
Paper accepted: November 22, 2022